AUTOMATED FLAW DETECTION USING UNRECONSTRUCTED COMPUTED TOMOGRAPHY DATA

J.D. Goldstein, W.G. Heller, J.A. Sivak, and J.V. White

The Analytic Sciences Corporation
55 Walkers Brook Drive
Reading, MA 01867

INTRODUCTION

Advances in aerospace materials and the need to apply these materials to perform near their structural limits requires new approaches to accurately determine material composition and state, and most importantly, reliably predict service life. Unfortunately most Nondestructive Evaluation (NDE) procedures are manual in nature (even though the sensors employed may be sophisticated), particularly during the data interpretation phase. For large structures like rocket motors or aircraft fuselage elements, the amount of NDE data which must be examined to assure safety is enormous. Even with tools such as x-ray tomography, an inspector must intently study the reconstruction imagery using full concentration over long periods of time. Often problems or flaws must be identified which lie at the limits of geometrical resolution, density resolution or both. Attempts to automate this process have been frustrated by both the critical nature of the task (no machine-based approach has come close to earning confidence) and the difficulty in formulating sufficiently robust detection algorithms which account for the wide variety of manufacturing tolerances, yet maintain the specificity of a human observer without a large false alarm rate.

In this paper, an approach is formulated and feasibility analysis is presented which quantifies the flaw detection problem to a degree that makes plausible the "inspector's helper" concept presented in Fig. 1. A human inspector observes a display of the test object's cross section as reconstructed from the x-ray data (this process is represented by the solid lines in the figure). However, using the same data and a systemized representation of the nominal dimensions and material content of the test article, the flaw detector (information flow indicated by dotted lines in the figure) highlights locations on the operators' display which deserve special inspection scrutiny. A reliably operating automated detection algorithm with a low false alarm rate (less than 3×10^{-6}) will speed up tedious inspection processes several fold. More importantly, the chances of not observing an important flaw will be nearly eliminated.

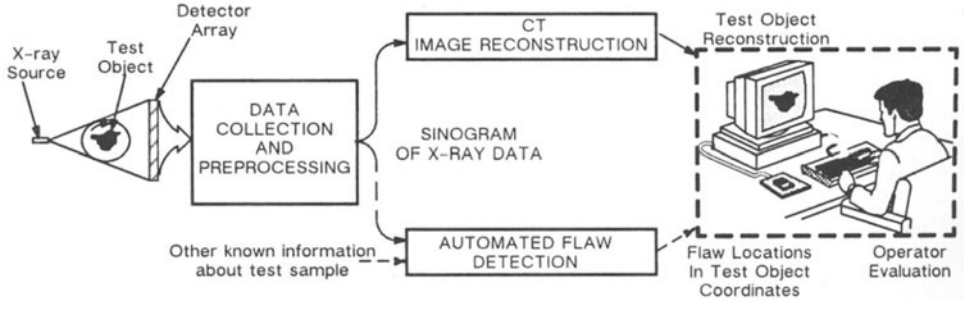

Figure 1 Mechanization of Automated X-Ray CT Flaw Detection

Review of Progress in Quantitative Nondestructive Evaluation, Vol. 9
Edited by D.O. Thompson and D.E. Chimenti
Plenum Press, New York, 1990

This paper presents an algorithm which assesses whether or not the density of any given volume element (voxel) of a test object is intended or not. The approach utilizes: x-ray scan data in sinogram form, a reference model for the nominal absorption of the x-ray beams by the test object, and error models for noise and drift in the measured data. By performing flaw *detection* (a two valued output process) rather than *reconstruction* (a multi-valued output process for gray scale image formation), more advantage is taken of the redundancy in the data (i.e., all x-rays passing through a single voxel are processed to directly strengthen the decision process).

Although the optimal selection and data combination theory presented herein is applied to the primitives from which x-ray computed tomographic (CT) imagery is normally reconstructed, the techniques are generally applicable to any NDE technique which provides a quantitative output describing the test object. The only requirement is that the test object be mathematically well-defined and that the dimensional and compositional uncertainties can be modeled.

Central to the automatic flaw detection scheme is a fully-formulated, totally quantitative theory of optimal detection using maximum likelihood techniques. In addition, means for testing and calibrating this approach are presented. Results based on actual CT scan data as well as simulations involving artificial CT scan data are also described.

ALGORITHM FORMATION

The mathematical basis of the flaw detection algorithm is provided in this section. First, a mathematical model is presented for the x-ray scan data. Then the flaw detection problem is stated precisely using this model. Finally, the flaw detection algorithm – the optimal solution of the detection problem – is described.

Data Model

The "raw" data from a CT scanner is represented as a sinogram. The sinogram is a rectangular matrix; the number in the i^{th} row and j^{th} column is the measured x-ray attenuation along a line of sight relative to the test object having angle θ_i and position r_j (as depicted in Fig. 2) with $0 \leq \theta_i < 180°$, and $r_{min} \leq r_j \leq r_{max}$.

The test object is modeled as consisting of n different species of material. The average attenuation of x-ray log intensity per unit distance of the

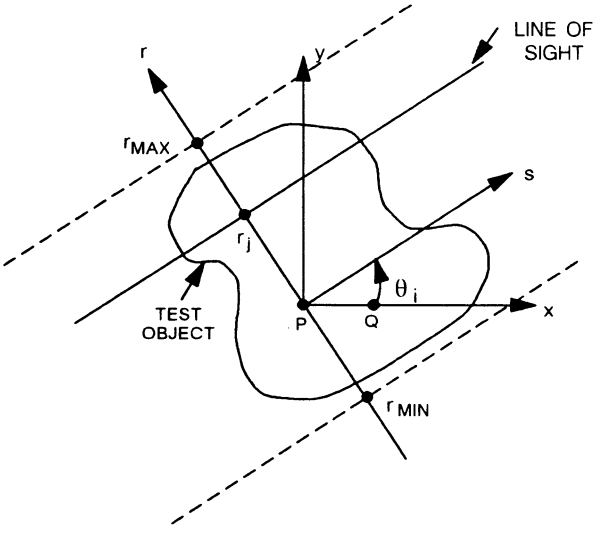

Figure 2 Line of sight parallel to s axis is defined by the i^{th} viewing angle θ_i (relative to a reference line PQ fixed to the test object) and the j^{th} position r_j (from reference point P). Point P is the origin of both the rs beam coordinate system and the xy object coordinate system.

k^{th} species, i.e., the attenuation coefficient, is denoted x_k and is measured in arbitrary computer tomography attenuation units per millimeter (CT/mm). The k^{th} x-ray projection measurement, z_k, is the observed x-ray attenuation in CT attenuation units along a specified line of sight. This measurement is modeled as the sum of three terms:

$$z_k = \hat{z}_k + a(x,y) + v_k \tag{1}$$

where $\hat{z}_k$ is the attenuation (without flaws) based on the geometry of the test object, $a(x,y)$ is the change in attenuation caused by a flaw at position (x,y) intercepted by the beam (when there is no flaw, $a(x,y) = 0$)), and v_k is the measurement noise.

The attenuation based on geometry, $\hat{z}_k$, is expressed as the sum of the products of the path length through each species times the corresponding attenuation coefficient of each species. In matrix notation:

$$z_k = H_k x \tag{2}$$

where x is the $n \times 1$ state vector of attenuation coefficients ($x = [x_1\ x_2\ \ldots\ x_n]^T$), and H_k is the $1 \times n$ geometry matrix that specifies the distance traveled by the x-ray beam through each species for the k^{th} measurement:

$$H_k = (H_{k1}\ H_{k2}\ \ldots\ H_{kn}) \tag{3}$$

In Eq. 3, H_{kj} denotes the distance traveled by the x-ray beam during the k^{th} measurement through the j^{th} species. The elements of H_k are determined using prior information about the test object (engineering specifications and prior geometric calibration data).

The state vector x is modeled as a normally distributed random vector having the prior mean vector $\hat{x}_1$ and the $n \times n$ prior covariance matrix P_1, i.e., $x \sim N[\hat{x}_1, P_1]$. The expected attenuation coefficients in $\hat{x}_1$ are determined from prior attenuation data for the materials comprising the test object. The covariance matrix P_1 is selected to model the unknown departures of the actual attenuation coefficients in x away from the expected values in $\hat{x}_1$.

The measurement noise v_k is modeled as a zero-mean, normally-distributed random variable with variance R_k, which varies from one measurement to the next (because the root-mean-square (rms) measurement noise in log-intensity measurements is nearly proportional to the attenuation). Different measurements are modeled as having independent noise and, therefore, the expected value of the product $v_j v_k$ is zero for $j \neq k$. Moreover, v_k is modeled as independent of the state vector x of attenuation coefficients. The value of R_k, expressed in terms of the expected attenuation based on geometry ($H_k\hat{X}_1$), the rms noise level (σ_1) of measurements that have been normalized with respect to the expected attenuations, and the rms level of additive noise (σ_2) is given by:

$$R_k = (\sigma_1 H_k \hat{x}_1)^2 + \sigma_2^2 \tag{4}$$

Flaw Detection Problem

The detection approach is to perform a statistical hypothesis test using all attenuation measurements whose beams intersect the voxel being considered (at position (x,y)). Two hypotheses are considered: (1) there is no flaw in the voxel, i.e., $a(x,y) = 0$; (2) there is a flaw in the voxel, i.e, $a(x,y) = \hat{a}$, where $\hat{a}$ is that value of flaw-induced attenuation for which the observed measurements are most probable (i.e., $\hat{a}$ is the maximum-likelihood estimate of $a(x,y)$). A precise statement of the detection problem follows:

Given the following model for attenuation data $z = (z_1\ z_2\ \ldots\ z_p)$ – whose beams intersect the voxel at position (x,y):

$$z_k = H_k x + a(x,y) + v_k \tag{5}$$

$$H_k = \text{matrix of path lengths} \tag{6}$$

$$x = \text{vector of attenuation coefficients} \sim N[\hat{x}_1, P_1] \tag{7}$$

$$\hat{x}_1 = \text{prior expected value of } x \tag{8}$$

$$P_1 = \text{prior covariance matrix of } x \tag{9}$$

$$a(x,y) = \text{flaw-induced attenuation} \tag{10}$$

v_k = white Gaussian measurement noise ~ $N[0, R_k]$ (11)

$R_k = (\sigma_1 H_k \hat{x}_1)^2 + \sigma_2^2$ (12)

σ_i = rms noise levels, i=1,2, (13)

and the two hypotheses:

H_0 = null hypothesis that there is no flaw (a(x,y) = 0)

H_1 = hypothesis that there is a flaw at position (x,y) in the test object, and a(x,y) = $\hat{a}$, which is the maximum-likelihood estimate of a(x,y),

Find an optimal decision rule for correctly choosing between hypotheses H_0 and H_1.

The optimality condition is to maximize the probability of correct detection for a specified probability of false alarm. The solution is to compute the probability odds ratio favoring H_1 over H_0 using all the relevant measurements z:

$$\text{odds ratio} = \frac{\text{Likelihood of } H_1}{\text{Likelihood of } H_0} \tag{14}$$

Select hypothesis H_1 when the odds ratio > threshold value.
Select hypothesis H_0 when the odds ratio $\leq$ threshold value.

Algorithm Implementation

Using Kalman-filtering theory [1], it can be shown that a sufficient statistic (which is equivalent to the odds ratio) for optimally detecting a flaw at position (x,y) in the test object is:

$$y = c \sum_{k=1}^{p} \frac{z_k - H_k \hat{x}_k}{H_k P_k H_k^T + R_k} \qquad \text{where} \qquad c = \sum_{k=1}^{p} \frac{1}{H_k P_k H_k^T + R_k} \tag{15) (16}$$

and each estimated state vector $\hat{x}_k$ and its covariance P_k at step k are computed from the gain matrix K_k using the following recursive algorithm:

$$K_k = P_k H_k^T [H_k P_k H_k^T + R_k]^{-1} \tag{17}$$

$$P_{k+1} = [I - K_k H_k] P_k \tag{18}$$

$$\hat{x}_{k+1} = \hat{x}_k + K_k [z_k - H_k \hat{x}_k] \tag{19}$$

In Eqs. 17-19, H_k^T denotes the matrix transpose of H_k, and I is the n × n identity matrix. The y statistic is a normally distributed random variable according to the data model, and under the null hypothesis H_0, y ~ N[0, 1]. A very important fact about this algorithm is that the matrices $\{K_k\}_{k=1}^{p}$, $\{P_k\}_{k=1}^{p}$ and $\{R_k\}_{k=1}^{p}$ can be precomputed off-line using Eqs. 12, 17 and 18. Later, when the attenuation measurements z_k become available, the flaw-detection algorithm processes them using Eq. 19 to compute the updated estimates $\{\hat{x}_k\}_{k=1}^{p}$ of the state vector x.

If $\hat{a} < 0$, e.g., the flaw has a low density, the optimal detector declares a flaw when the y statistic is less than a threshold (y < - T), and if $\hat{a} > 0$, the optimal detector declares a flaw when y > T. These are one-sided hypothesis tests, and it is straightforward to determine that detection threshold, T, which corresponds to any desired false-alarm probability P_f.

Calibration

The automated flaw detection algorithm described above is appropriate when uncertainties about the attenuation coefficients in vector x, the path lengths in H_k, and the rms noise levels σ_1 and σ_2 (see Eq. 12) are small enough to achieve separation between unflawed measurements and the detection threshold.* To achieve this degree of certainty, it is necessary to perform a

*Note that this condition is also necessary if a human inspector is to have any hope of distinguishing flaws manually in a reconstructed image.

calibration prior to flaw detection. This calibration uses available geometric information about the dimensions of the test object and information about the attenuation coefficients of each material species. The calibration also uses the sinogram data that are input to the flaw detection algorithm.

The rms noise level σ_1 is determined by using data from adjacent rows in the sinogram. Let z_i be a vector of the attenuation measurements (an attenuation profile) from the row corresponding to angle θ_i. From prior information about the test object, these rows may be selected so that the two attenuation profiles differ from each other primarily because of measurement noise. From these profiles, a normalized noise vector $n = [n(1)n(2) \ldots]$ is computed:

$$n(k) = \frac{z_i(k) - z_{i+1}(k)}{z_i(k) + z_{i+1}(k)} \tag{20}$$

The vector n is treated as a time series, and a spectral analysis yields its noise content. From the power spectrum of n, the high-frequency rms noise level in the sinogram is specified. The output of this analysis is an accurate determination of the rms measurement noise σ_1 for use in the flaw-detection algorithm.

The second rms noise level, σ_2, models the relatively small additive noise (that is clearly observed in measurements corresponding to rays that do not intersect the test object). Let z_k denote a column of data from the sinogram (containing p measurements) that corresponds to rays which do not intersect the test object. The residuals of the measurements are given by (for $j = 1, 2, \ldots, p$)

$$\delta z_k(j) = z_k(j) - m_k \tag{21}$$

where m_k is the mean of the measurements. The value of σ_2 is given by the standard deviation of these residuals:

$$\sigma_2 = \sqrt{\frac{1}{p} \sum_{j=1}^{p} \delta z_k(j)^2} \tag{22}$$

THEORETICAL PERFORMANCE ANALYSIS

The ability of the flaw detection algorithm to detect a flaw-induced attenuation change of magnitude a(x,y) can be measured in terms of the probability of detection (P_d), the probability of false alarm (P_f), and the average signal-to-noise ratio (SNR) of the attenuation measurements. Plotting P_d as a function of P_f for different SNRs yields what is known in detection theory as the Receiver Operating Characteristic (ROC) of the algorithm. This is a plot of performance trade-off curves showing how P_d can be traded for P_f.

The theoretical ROC plot for the algorithm, as currently formulated, is shown in Fig. 3. The vertical dashed line at $P_f = 3 \times 10^{-6}$ corresponds to less than one false alarm per 512 x 512 voxels. It intersects the curve for SNR = -6 decibels (dB) at $P_d = 0.99$. This shows that (with the detection threshold set high enough so that, on the average, one false alarm occurs only every 330,000 voxels) a flaw-induced density corresponding to SNR = -6 dB will be detected with a probability of 0.99. The SNR in decibels is defined as

$$SNR = 10 \log_{10} \frac{a(x,y)^2}{R_k} \tag{23}$$

Therefore, -6 dB means that the flaw-induced attenuation is one half of the average rms noise level in the sinogram data. This SNR corresponds to one-voxel air voids at the resolution limit of the sinogram and a higher noise level than that observed in real sinogram data provided by Aracor, Inc. for an aluminum-disk test object. The conclusion to be drawn from this analysis is that "point" flaws are reliably (99%) detectable with very small false-alarm probabilities (3×10^{-6}). This P_f corresponds to less than one false alarm in an entire reconstructed cross section which fills a 512 x 512 pixel workstation screen.

CT DATA SIMULATOR

To verify the correctness of the software implementation and to confirm the statistical behavior of the flaw detection algorithm, a CT simulator was

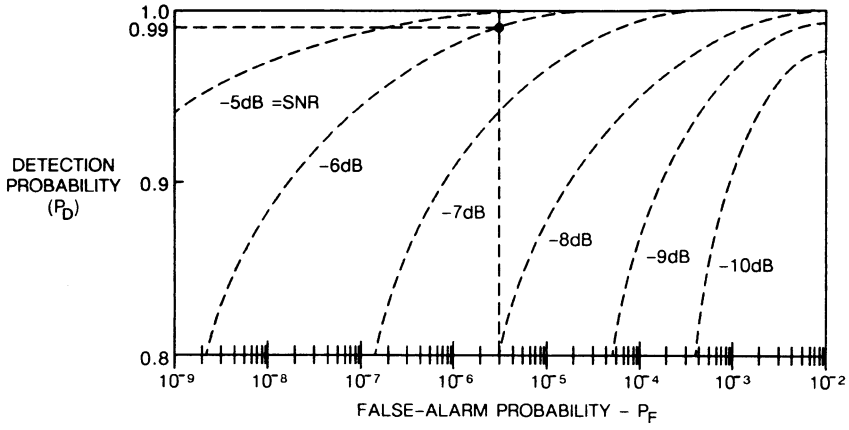

Figure 3 Theoretical ROC for the Automatic Flaw Detection Algorithm

implemented. The simulator models an ideal object, a solid of precisely defined shape and composition, which may be made to contain flaws of known dimensions at known locations, e.g., a "phantom" [2,3,4].

Measurement noise is added to the simulated sinogram measurements to account for random fluctuations in the x-ray beam intensity and detector outputs. If $\hat{Z}(\theta_i, r_j)$ denotes the noise-free attenuation for the line-of-sight identified by the pair (θ_i, r_j) then $Z(\theta_i, r_j)$, the corresponding simulated measurement, is given by:

$$Z(\theta_i, r_j) = (1 + w_{ij})\hat{Z}(\theta_i, r_j) + n_{ij} \tag{24}$$

where w_{ij} and n_{ij} are normal variates, independent from point to point, with zero mean and standard deviation σ_1 and σ_2 respectively. These noise terms are consistent with Eqs. 4, 20, and 22. For the sinogram used in the algorithm tests, $\sigma_1 = 0.024$ and $\sigma_2 = 15.2$ attenuation units. These values were estimated from Aracor data using the methodology previously described.

The effect of measurement noise can easily be seen on a slice through the sinogram. Figure 4a shows the section through the generated sinogram corresponding to fixed angle $\theta_i = 0$. It presents the simulated attenuation, $Z(0, r_j)$, for parallel horizontal x-ray beams at varying distances from the center. Note that the noise fluctuations are large near the center where the attenuation values are high, and small near the edges of the disk, where the attenuation is the lowest. For comparison purposes, Fig. 4b shows the same slice through the Aracor sinogram.

NUMERICAL FEASIBILITY RESULTS

The performance of the automated flaw detection algorithm was demonstrated using simulated CT scan data. The parameters of the data are matched to those of real scan data provided by Aracor, Inc. for a 10 cm diameter aluminum-disk test object. Standard tomographic reconstruction and image enhancement techniques applied to these data failed to highlight four 0.5mm diameter air voids. In contrast, the results presented here demonstrate that these extremely small flaws are readily detectable with the automated flaw-detection algorithm, which works directly on scan data independently of any reconstruction procedure.

Two rms noise levels are simulated: one equal to the noise level in the Aracor data; another which is twice that rms noise level. The results of applying the detection algorithm to the simulated scan data in 36 Monte Carlo trials are presented in Table 1 for data containing flaws and in Table 2 for data containing no flaws. The normalized detection threshold (T) of the detector is set to 4.5 so that the false-alarm probability P_f is 3×10^{-6}. (The probability is 3×10^{-6} that $|y|>4.5$ standard deviations by random chance alone when the flaw is absent.) The detection algorithm outputs "flaw present" when the normalized detection statistic $|y|>T$; otherwise the output is "flaw absent."

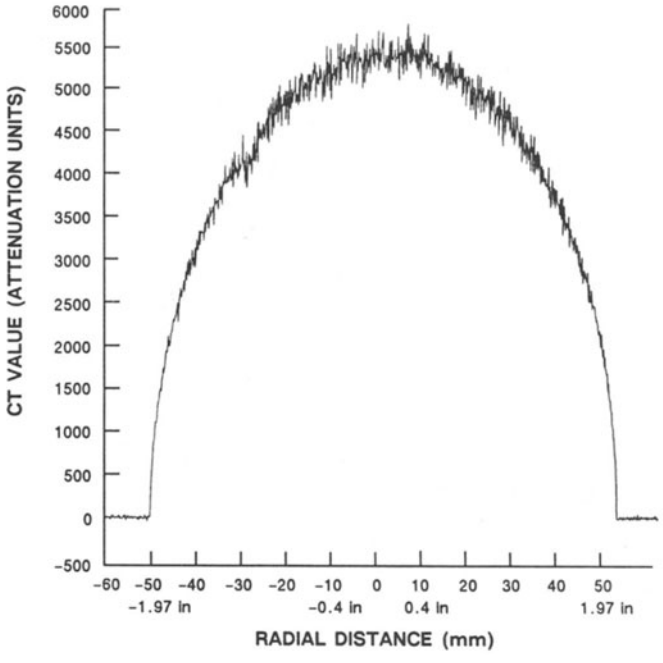

Figure 4a Synthetic Sinogram for $\theta = 0$

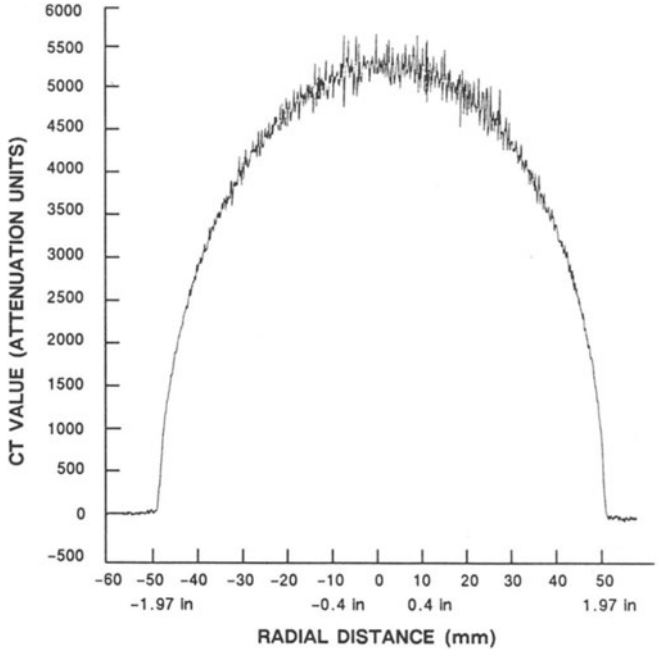

Figure 4b Actual Sinogram for $\theta = 0$ (Data provided by Aracor, Inc.)

Table 1 Monte Carlo Trials with 0.5mm Flaw Present

TRIAL NUMBER	RMS NOISE LEVEL (relative to Aracor data)	DETECTION STATISTIC (y)	DETECTOR OUTPUT
1	1.0	10.3	flaw present
2	1.0	10.8	flaw present
3	1.0	11.0	flaw present
4	1.0	13.4	flaw present
5	1.0	12.7	flaw present
6	1.0	13.5	flaw present
7	1.0	13.1	flaw present
8	1.0	13.2	flaw present
9	1.0	11.3	flaw present
10	2.0	9.0	flaw present
11	2.0	14.0	flaw present
12	2.0	9.0	flaw present
13	2.0	10.5	flaw present
14	2.0	11.9	flaw present
15	2.0	14.3	flaw present
16	2.0	14.5	flaw present
17	2.0	13.7	flaw present
18	2.0	10.4	flaw present

Table 2 Monte Carlo Trials with Flaw Absent

TRIAL NUMBER	RMS NOISE LEVEL (relative to Aracor data)	DETECTION STATISTIC (y)	DETECTOR OUTPUT
19	1.0	0.02	flaw absent
20	1.0	0.15	flaw absent
21	1.0	1.28	flaw absent
22	1.0	0.24	flaw absent
23	1.0	0.46	flaw absent
24	1.0	0.51	flaw absent
25	1.0	0.56	flaw absent
26	1.0	0.48	flaw absent
27	1.0	0.89	flaw absent
28	2.0	0.09	flaw absent
29	2.0	0.35	flaw absent
30	2.0	2.56	flaw absent
31	2.0	0.38	flaw absent
32	2.0	0.91	flaw absent
33	2.0	0.95	flaw absent
34	2.0	1.10	flaw absent
35	2.0	0.86	flaw absent
36	2.0	1.70	flaw absent

Examination of Table 1 shows that the algorithm reliably detects 0.5mm flaws as expected. In each trial the 0.5mm flaw is detected. It is noteworthy that the detection statistic $|y|$ exceeds the threshold of 4.5 by a factor of at least 2 in all trials, even when the noise is twice the level observed in the Aracor scan data. Likewise, Table 2 verifies that the algorithm produces the appropriate null output in all trials when there is no flaw in the test object. This result is consistent with the extremely low false-alarm probability of 3×10^{-6}.

CONCLUSIONS AND SUMMARY

A new approach to flaw detection, which quantitatively accounts for all available information about a test object, including prior information about nominal size, composition and uncertainty is presented. Initial development and testing of the approach using actual and simulated CT x-ray scan data indicates that small flaws can be reliably detected under realistic inspection conditions. In simulation test results, detectability resolution limit of the algorithm was approximately a factor of two smaller (single linear dimension) than the visual detectability limit in the reconstructed image.

ACKNOWLEDGEMENTS

This work was supported by the Center for NDE at Iowa State University under Contract No. SC-88-146. Encouragement by D. Chimenti of the Air Force Materials Laboratory and by D. Thompson of the Center was an important contribution to this work. Data provided by the Aracor Corporation is gratefully acknowledged.

REFERENCES

1. Gelb, A. (Ed.), Applied Optimal Estimation, MIT Press, Cambridge, 1974.
2. Shepp, L.A., and Logan, B.F., "The Fourier Reconstruction of a Head Section," IEEE Trans. Nucl. Sci., Vol. 21, pp. 21-43, 1974.
3. Herman, G.T., and Rowland, S.W., "SNARK77: A Programming System for Image Reconstruction from Projections," Report No. 130, Dept. of Computer Science, State University of New York at Buffalo, Amherst, New York, 1978.
4. Herman, G.T., Image Reconstruction from Projections, Academic Press, New York, 1980.